RSC Advances

PAPER

View Article Online
View Journal | View Issue

Synthesis of highly efficient and recyclable visible-light responsive mesoporous g-C_3N_4 photocatalyst *via* facile template-free sonochemical route†

Cite this: *RSC Adv.*, 2014, **4**, 8132

Santosh Kumar,[a] T. Surendar,[a] Bharat Kumar,[b] Arabinda Baruah[b] and Vishnu Shanker*[a]

Received 26th July 2013
Accepted 27th November 2013

DOI: 10.1039/c3ra43942a

www.rsc.org/advances

Herein we demonstrate a facile template-free sonochemical strategy to synthesize mesoporous g-C_3N_4 with a high surface area and enhanced photocatalytic activity. The TEM and nitrogen adsorption–desorption studies confirm mesoporous structure in g-C_3N_4 body. The photocatalytic activity of mesoporous g-C_3N_4 is almost 5.5 times higher than that of bulk g-C_3N_4 under visible-light irradiation. The high photocatalytic performance of the mesoporous g-C_3N_4 was attributed to the much higher specific surface area, efficient adsorption ability and the unique interfacial mesoporous structure which can favour the absorption of light and separation of photoinduced electron–hole pairs more effectively. A possible photocatalytic mechanism was discussed by the radicals and holes trapping experiments. Interestingly, the synthesized mesoporous g-C_3N_4 possesses high reusability. Hence the mesoporous g-C_3N_4 can be a promising photocatalytic material for practical applications in water splitting as well as environmental remediation.

1. Introduction

Graphitic carbon nitride (g-C_3N_4) a typical metal-free polymeric semiconductor material has attracted a great deal of scientific interest due to its suitable band gap to absorb the visible-light and unique properties.[1] The g-C_3N_4 is considered the most stable allotrope in ambient conditions. The structure stability and redox ability of g-C_3N_4 semiconductor stimulate us to explore its application as a new metal-free photocatalyst that directly splits water or degrades environmental pollutants under visible-light irradiation. Some studies have been focused on the applications of g-C_3N_4 in water splitting and degradation of organic pollutants under visible light irradiation.[2,3] However, the efficiency of this metal-free polymeric photocatalyst (g-C_3N_4) is still limited due to the high recombination rate of photogenerated electron–hole pairs, and low surface area which is insufficient for visible-light absorption.[4] More recently, several efforts have been made to improve the photocatalytic activity of g-C_3N_4 by employing different modifications such as loading co-catalyst onto the surface of g-C_3N_4, designing appropriate textural properties, doping and making composites with other semiconductor materials.[5–8]

However, the major drawback of bulk g-C_3N_4 is that the high degree of polycondensation of monomers during the synthesis process at 550 °C makes the resulting g-C_3N_4 materials with low surface area (less than 10 $m^2 g^{-1}$), without forming textured pores.[1] In general large surface area is a basic need for a heterogeneous catalyst to be chemically productive *via* offering more surface reactive sites, improving mass transfer, and enhancing light-harvesting. Moreover, the diffusion path of photoinduced electron–hole pair from the bulk to the surface inside high surface area materials is short. Therefore, recombination during the transfer is greatly suppressed in such material.[3] Such a surface effect has been known recently for g-C_3N_4 and also for TiO_2.[3,9]

To date, there are few reports on the synthesis of porous graphitic carbon nitride. Recently, Vinu *et al.* reported the synthesis of mesoporous g-C_3N_4 with a uniform pore diameter using SBA-15 as a template,[10] but the carbon to nitrogen (C/N) ratio is high (3.3–4.5), making this material more like a nitrogen-doped carbon. Chen *et al.* has also applied a templating route to yield ordered mesoporous g-C_3N_4 and studied its activity towards water splitting under visible light irradiation.[11] In this work, we report a facile template free sonochemical approach for the synthesis of mesoporous g-C_3N_4 photocatalyst at ambient temperature. Our results demonstrate that mesoporous g-C_3N_4 shows enhanced photocatalytic performance for degradation of RhB under visible-light irradiation.

[a]*Department of Chemistry, National Institute of Technology, Warangal-506004, A.P., India. E-mail: vishnu@nitw.ac.in; Fax: +91-870-2459547; Tel: +91-870-2462675*

[b]*Department of Chemistry, Indian Institute of Technology Delhi, New Delhi-110016, India*

† Electronic supplementary information (ESI) available. See DOI: 10.1039/c3ra43942a

2. Experimental section

2.1 Materials and method

Bulk g-C_3N_4 was prepared by naturally heating melamine (Sigma-Aldrich, 99.0%) to 550 °C for 2 h in N_2 atmosphere.[12] Mesoporous g-C_3N_4 was prepared by dissolving 0.1 g of bulk g-C_3N_4 in 150 mL of ethanol–water (1 : 2) and sonicated (PCI analytics, probe: 12 mm, 33 Hz, 150 watts) for 5 h at ambient temperature. The powder was collected by centrifugation, washed with deionized water, and dried in an oven at 100 °C.

2.2 Characterization

Powder X-ray diffraction studies (PXRD) were carried out on a Bruker D_8 Advance diffractometer. The FTIR spectra were recorded in transmission mode from 4000 to 400 cm^{-1} on a Nicolate Protégé 460 FTIR spectrometer using KBr discs. TEM was done on a JEOL, JSM-6700F instrument. SEM-EDX was done on a VEGA3, TESCAN instrument. UV-Vis diffuse reflectance spectra were recorded on a Lambda/20 Instrument (UV-Vis NIR spectrophotometer), equipped with an integrating sphere to record the diffuse reflectance spectra of the samples, and $BaSO_4$ was used as a reference. Nitrogen adsorption–desorption isotherm was carried out by using Quanta chrome NOVA 1200e. The photoluminescence (PL) spectra were recorded on TSC solutions F96PRO fluorescence spectrophotometer with excitation wavelength of 365 nm.

2.3 Photocatalytic activity

The photocatalytic activity of mesoporous g-C_3N_4 (50 mg) was evaluated for degradation of rhodamine (RhB) solution (5 mg L^{-1}, 100 mL) in a beaker with constant stirring under visible light. The visible-light source for the photo-irradiation is solar simulator 300 W Xe lamp (Asahi Spectra Co., Ltd) with a super cold filter, which provides the visible light region ranging from 400 nm to 700 nm and a light intensity of 115 mW cm^{-2}. Prior to irradiation, photocatalysts were suspended in the solutions with constant stirring under dark conditions for 30 min to ensure that the surface of catalyst was saturated with RhB. During photocatalysis processes, the catalyst was periodically withdrawn (sampling time of 5 min), centrifuged to separate the catalyst powder from the solution, and used for the absorbance measurement. The absorption spectra were recorded on a UV-Vis spectrophotometer. The photocatalytic activity of mesoporous g-C_3N_4 was compared with the bulk g-C_3N_4 under the same experimental conditions.

2.4 Detection of reactive species

Reactive oxidative species detection process is similar to the photodegradation experimental process. Various scavengers were subjected into the RhB solution prior to addition of photocatalyst. Furthermore, photoluminescence (PL) spectra with terephthalic acid (TA) as a probe molecule were used to disclose the formation of $^{\bullet}OH$ radicals on the surface of mesoporous g-C_3N_4 under visible-light irradiation. In a brief experimental procedure, photocatalyst (0.1 g) was dispersed in 40 mL of the TA (5×10^{-4} mol L^{-1}) aqueous solution with NaOH (2×10^{-3} mol L^{-1}) at room temperature. The above suspension was subjected, for the photocatalytic activity evaluation of the photocatalyst, to visible-light irradiation and the PL intensity measured using a fluorescence spectrophotometer with excitation wavelength of 365 nm.

3. Results and discussion

3.1 Catalyst characterization

The X-ray diffraction (XRD) patterns of bulk and mesoporous g-C_3N_4 photocatalysts are shown in Fig. 1a. The results indicate that a diffraction peak at 27.54 appears in both bulk and mesoporous g-C_3N_4 which corresponds to the (002) plane of g-C_3N_4.[1]

The FTIR spectra of bulk and mesoporous g-C_3N_4 photocatalysts is shown in Fig. 1b. The broad bands around 3100 cm^{-1} indicate N–H stretching vibrations, the peaks at 1243 cm^{-1} and 1637 cm^{-1} correspond to the C–N and C=N stretching vibrations, respectively. The peak at 808 cm^{-1} was related to the *s*-triazine ring vibrations.[13–15] All characteristic peaks of g-C_3N_4 were observed in mesoporous g-C_3N_4.

The morphology of the as synthesised photocatalysts was investigated by transmission electron spectroscopy (TEM). Fig. 2 shows the TEM images of mesoporous g-C_3N_4. As can be seen from Fig. 2a and b, the synthesized g-C_3N_4 possesses a mesoporous structure. The textural mesopores were also seen in the TEM image and average pore diameter 7 nm. These findings are in good agreement with the results obtained from N_2-adsorption measurements. TEM image of bulk g-C_3N_4 is shown in Fig. S1.† SEM-EDX was further used to determine the presence of carbon and nitrogen in the bulk and mesoporous g-C_3N_4 photocatalysts (Fig. 3). The carbon to nitrogen (C/N) ratio is found to be 0.77 for bulk g-C_3N_4 and 0.85 for mesoporous g-C_3N_4.

UV-Vis diffuse reflectance measurements of bulk and mesoporous g-C_3N_4 are shown in Fig. 4a. The slight blue shift in the band edge positions to lower wavelength in mesoporous g-C_3N_4 (463 nm) as compared with bulk g-C_3N_4 (470 nm) is due to the increase in carbon to nitrogen ratio of mesoporous g-C_3N_4 which making this material like a nitrogen-doped N doped g-C_3N_4. Therefore, the mesoporous g-C_3N_4 can show a stronger optical absorption than bulk g-C_3N_4, in the visible region.

The specific surface area and pore size distribution of bulk g-C_3N_4 and mesoporous g-C_3N_4 were investigated by nitrogen adsorption–desorption analysis (Fig. 4b). The shape of the adsorption isotherm in Fig. 3b of the mesoporous g-C_3N_4 is a clear example of a type IV isotherm characteristic of mesoporous materials. From Table 1 it is observed that the calculated specific surface area and pore volume of the synthesized mesoporous g-C_3N_4 were much higher than that of bulk g-C_3N_4, respectively. Pore size distributions determined by the BJH Method (Fig. S2†). The average pore diameter is 7.1 nm for mesoporous g-C_3N_4. The high surface area, mesoporous structure, and large pore volume indicate that this mesoporous g-C_3N_4 will be an interesting porous semiconductor material for further study in environmental applications.

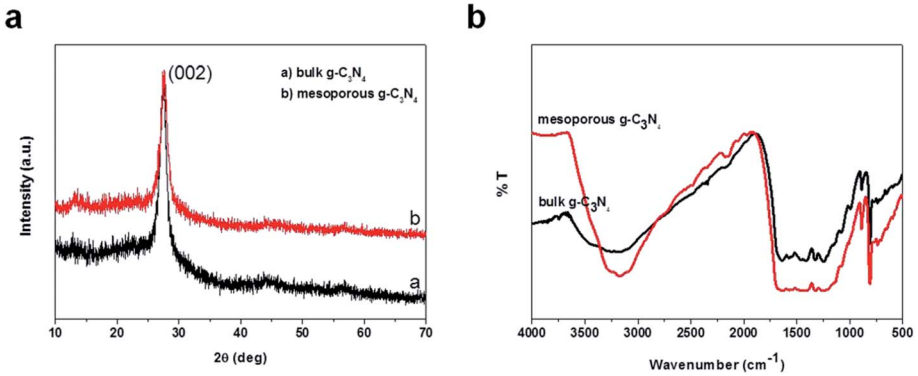

Fig. 1 XRD pattern (a) and FTIR (b) of the synthesized bulk and mesoporous g-C_3N_4.

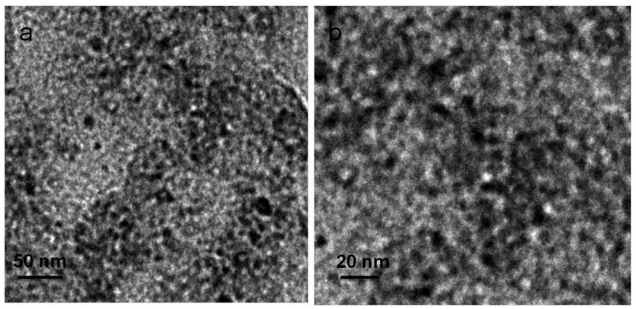

Fig. 2 TEM images of the synthesized mesoporous g-C_3N_4: (a) mesoporous g-C_3N_4 (b) mesoporous g-C_3N_4 (magnified).

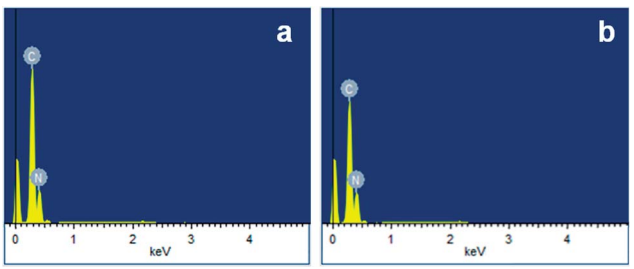

Fig. 3 SEM-EDX of the synthesized bulk and mesoporous g-C_3N_4.

3.2 Photocatalytic activity

Photocatalytic activity of the synthesized samples was evaluated *via* photodegradation of RhB under visible-light irradiation. The absorption of spectra of bulk and mesoporous g-C_3N_4 is shown in Fig. S3.† To disclose the efficiency of photocatalyst, the adsorption ability of the synthesized catalyst was also examined in dark conditions under the same experimental conditions (Fig. S4).† Mesoporous g-C_3N_4 shows good adsorption ability towards RhB compared to bulk g-C_3N_4 under similar conditions which can enhance the photocatalytic activity as it is the first step of the photocatalytic process. Further, the blank test demonstrates that the irradiation without photocatalyst has no effect on the degradation process under the same experimental conditions, suggesting the presence of both catalysts and light irradiation is necessary for efficient degradation. Fig. 5a shows the comparison of photocatalytic activity for degradation of RhB over bulk and mesoporous g-C_3N_4 and TiO_2 (P25). The photocatalytic activity of mesoporous g-C_3N_4 is almost 5.5 times higher than that of bulk g-C_3N_4. The high photocatalytic activity may be governed by good adsorption ability, large surface area and high charge separation efficiency of photoinduced electron–hole pairs in mesoporous g-C_3N_4.

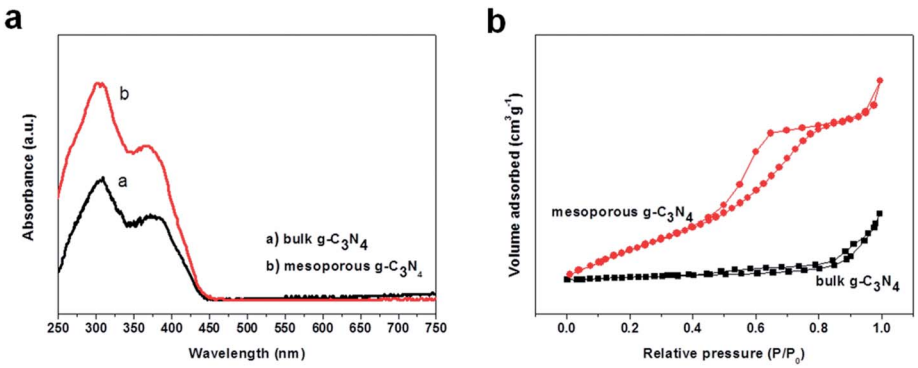

Fig. 4 UV-Vis DRS (a) and nitrogen adsorption–desorption isotherm (b) of the synthesized bulk and mesoporous g-C_3N_4.

Table 1 Textural and photocatalytic properties of the synthesized bulk and mesoporous g-C_3N_4

Sl no.	Photocatalyst	Surface area ($m^2\ g^{-1}$)	Pore volume ($cm^3\ g^{-1}$)	Pore diameter (nm)	Rate constant (sec^{-1})
1	Bulk g-C_3N_4	8.4	0.08	—	0.009
2	Mesoporous g-C_3N_4	112.38	0.39	7.1	0.050

3.3 Photoluminescence

Fig. 5b shows the PL spectra of bulk and mesoporous g-C_3N_4 excited at 365 nm at room temperature. Mesoporous g-C_3N_4 shows a broad PL peak at 465 nm. Compared to bulk g-C_3N_4, the PL intensity of mesoporous g-C_3N_4 was greatly suppressed, indicating the electron localization on the surface terminal sites. It is clearly seen that a porous network of g-C_3N_4 is useful to reduce the recombination rate of photoinduced electron–hole pairs and improves the corresponding photocatalytic activity.[16,17]

3.4 Detection of reactive oxidative species

In general, reactive oxygen species including $^{\bullet}OH$ and $O_2^{\bullet-}$ are expected to be involved in the photocatalytic process. To investigate the role of these reactive species, the effects of some radical scavengers and N_2 purging on the photodegradation of RhB were studied to propose the possible photocatalytic mechanism. As the photoinduced electron–hole pair separated in g-C_3N_4 photocatalyst, the photoinduced electron can directly produce $O_2^{\bullet-}$ from dissolved O_2 because the E_{CB} (g-C_3N_4, −1.3 eV *vs.* NHE) is lower than $E_{(O_2/O_2^{\bullet-})}$ (+0.13 eV *vs.* NHE), but $E_{(VB)}$ (g-C_3N_4, +1.4 eV *vs.* NHE) is also lower than $E_{(OH/H_2O)}$ (+2.68 eV *vs.* NHE), which cannot oxidize the adsorbed H_2O molecules to $^{\bullet}OH$ on the surface of g-C_3N_4. It can be seen from Fig. 6a, that when N_2 purging was conducted which acts as $O_2^{\bullet-}$ scavenger, a dramatic change in photocatalytic activity was observed compared with absence of scavenger, which confirms that the dissolved O_2 has a clear effect on the photodegradation process under visible-light irradiation. However, there was no change observed in the photocatalytic degradation of RhB by the addition ammonium oxalate (AO) as holes scavenger compared with no scavenger under similar conditions, indicating that the superoxide radicals followed by $^{\bullet}OH$ are the main active oxidative species of the mesoporous g-C_3N_4 photocatalyst and can play an important role in the photodegradation of RhB under visible-light irradiation, but not the holes. Moreover, photoluminescence (PL) technique was also employed to detect the formation of $^{\bullet}OH$. PL emission peak at about 425 nm of 2-hydroxyterephthalic acid was observed and gradually increased with the irradiation time, which indicates the formation of photoinduced $^{\bullet}OH$ under visible-light irradiation (Fig. 6b).

3.5 Recyclability

The recyclability of a photocatalyst is one of the important factors for practical applications. Interestingly the porous g-C_3N_4 photocatalyst can be easily recycled by simple filtration or centrifugation and further it can avoid the second pollution. To study the recyclability of porous g-C_3N_4 photocatalyst, five successive photocatalytic experiments were carried out by adding used porous g-C_3N_4 photocatalyst to fresh RhB solutions with no change in overall concentration of the catalyst under visible-light irradiation. The photocatalytic activity of porous g-C_3N_4 photocatalyst retains over 90% of its original activity after five successive experimental runs of invisible-light irradiation as shown in Fig. 7. The XRD studies were performed for reused mesoporous g-C_3N_4 photocatalyst (Fig. S5†) and no change was observed in the resulting spectra which indicates the high structural stability of porous g-C_3N_4. Therefore, g-C_3N_4 composites can be used as high-performance visible-light photocatalysts and their potential applications in environmental protection.

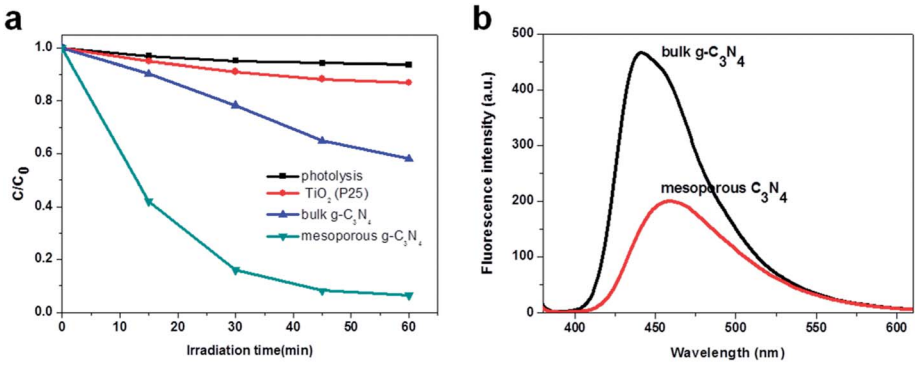

Fig. 5 Photocatalytic degradation of RhB in aqueous solution over bulk and mesoporous g-C_3N_4 (a), and room temperature photoluminescence (PL) spectra of bulk and mesoporous g-C_3N_4 excited at 365 nm (b).

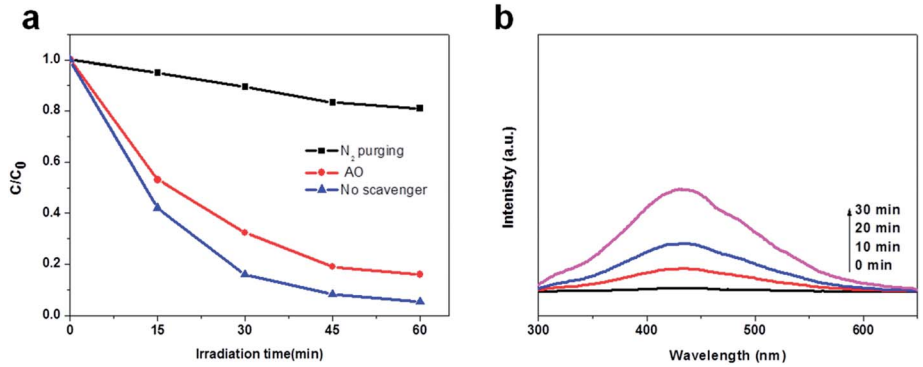

Fig. 6 Effects of different scavengers on degradation of RhB in the presence of mesoporous g-C_3N_4 catalyst under visible-light irradiation (a), and $^{\bullet}OH$ trapping PL spectra of g-C_3N_4 with TA solution under visible-light irradiation (b).

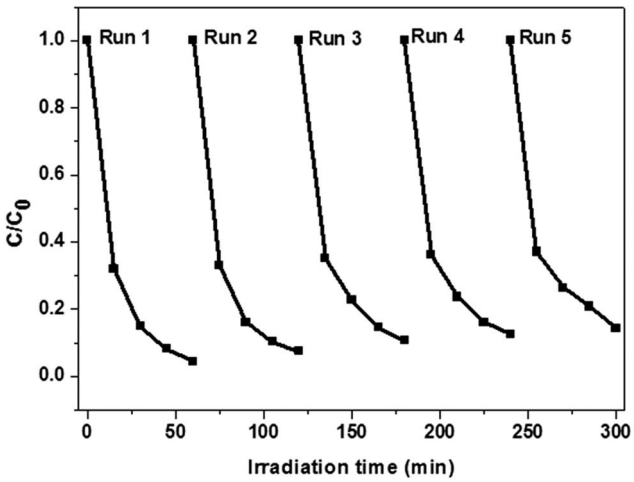

Fig. 7 Recyclability of mesoporous g-C_3N_4 photocatalyst in five successive experiments for photocatalytic degradation of RhB in aqueous solution under visible-light irradiation (no change in overall catalyst concentration for each run).

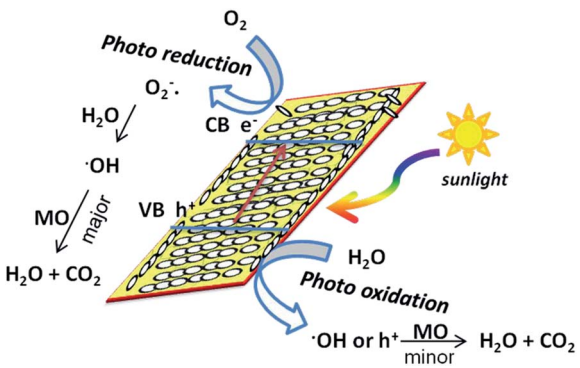

Fig. 8 Schematic diagram showing the process of the photocatalytic RhB degradation over the mesoporous g-C_3N_4.

3.6 Mechanism for improved performance

In general, the large surface area, high adsorption ability and improved charge separation can play an important role for the enhancement of photocatalytic activities.[12,18–21]

On the basis of the above results, a possible pathway has been discussed for the improved photocatalytic performance of the synthesized mesoporous g-C_3N_4 as shown in Fig. 8. It may be synergistic effects including high adsorption ability, large surface area and charge separation. First, it is well-known that the catalytic process is mainly related to the adsorption and desorption of molecules on the surface of the catalyst. The large surface area is useful for adsorption of organic compounds and further enhances efficiency of the photocatalytic process, as adsorption of organic compound on the surface of photocatalyst is the initial step of photocatalytic oxidation of organic compounds. In addition this large surface area provides a higher number of reactive sites for photocatalytic processes. Therefore, mesoporous g-C_3N_4 with high surface area can lead to better adsorption ability thereby enhancing photocatalytic performance. Second, a porous structure can provide more single sites and special passages for charge transport. Thus, the porous network in g-C_3N_4 photocatalyst may enhance photocatalytic reactivity under the visible-light irradiation, providing a promising strategy for the design and fabrication of novel photocatalysts with high performances. These above aspects together attributed for the improved photocatalytic performance of mesoporous g-C_3N_4.

4. Conclusion

In summary, we have demonstrated a facile template free sonochemical approach to synthesize mesoporous g-C_3N_4 sheet. Our results clearly indicate that the synthesized g-C_3N_4 sheet possesses the porous structure with high surface area and large pore volume. More attractively, the photocatalytic activity of mesoporous g-C_3N_4 is much higher compared to bulk g-C_3N_4 under visible-light irradiation. The reactive oxidative species detection studies indicated that the photodegradation of RhB over mesoporous g-C_3N_4 under visible-light is mainly *via* superoxide radicals. More importantly, the high reusability of the synthesized mesoporous g-C_3N_4 can meet the requirement of suitable candidates for practical photocatalytic applications.

Acknowledgements

Authors thank DST, Govt of India, for financial support (SR/FT/CS-096/2009). Santosh Kumar also thanks MHRD, Govt of India, for a fellowship.

References

1 X. Wang, K. Maeda, A. Thomas, K. Takanabe, G. Xin, J. M. Carlsson, K. Domen and M. Antonietti, *Nat. Mater.*, 2009, **8**, 76.
2 K. Maeda, X. C. Wang, Y. Nishihara, D. L. Lu, M. Antonietti and K. Domen, *J. Phys. Chem. C*, 2009, **113**, 4940.
3 X. C. Wang, K. Maeda, X. F. Chen, K. Takanabe, K. Domen, Y. D. Hou, X. Z. Fu and M. Antonietti, *J. Am. Chem. Soc.*, 2009, **131**, 1680.
4 S. C. Yan, Z. S. Li and Z. G. Zou, *Langmuir*, 2009, **25**, 10397.
5 J. Li, B. Shen, Z. Hong, B. Lin, B. Gao and Y. Chen, *Chem. Commun.*, 2012, **48**, 12017.
6 X. C. Wang, X. F. Chen, A. Thomas, X. Z. Fu and M. Antonietti, *Adv. Mater.*, 2009, **21**, 1609.
7 S. C. Yan, S. B. Lv, Z. S. Li and Z. G. Zou, *Dalton Trans.*, 2010, **39**, 1488.
8 G. S. Li, D. Q. Zhang and J. C. Yu, *Chem. Mater.*, 2008, **20**, 3983.
9 E. Martínez-Ferrero, Y. Sakatani, C. Boissiere, D. Grosso, A. Fuertes, J. Fraxedas and C. Sanchez, *Adv. Funct. Mater.*, 2007, **17**, 3348.
10 A. Vinu, K. Ariga, T. Mori, T. Nakanishi, S. Hishita, D. Golberg and Y. Bando, *Adv. Mater.*, 2005, **17**, 1648.
11 X. Chen, Y. S. Jun, K. Takanabe, K. Maeda, K. Domen, X. Fu, M. Antonietti and X. Wang, *Chem. Mater.*, 2009, **21**, 4093.
12 S. Kumar, T. Surendar, A. Baruah and V. Shanker, *J. Mater. Chem. A*, 2013, **1**, 5333.
13 M. J. Bojdys, J. O. Muller, M. Antonietti and A. Thomas, *Chem. - Eur. J.*, 2008, **14**, 8177.
14 Y. Zhao, D. Yu, H. Zhou, Y. Tian and O. Yanagisawa, *J. Mater. Sci.*, 2005, **40**, 2645.
15 X. Li, J. Zhang, L. Shen, Y. Ma, W. Lei, Q. Cui and G. Zou, *Appl. Phys. A: Mater. Sci. Process.*, 2009, **94**, 387.
16 J. D. Hong, X. Y. Xia, Y. S. Wang and R. Xu, *J. Mater. Chem.*, 2012, **22**, 15006.
17 P. Wang, B. Huang, Y. Dai and M. H. Whangbo, *Phys. Chem. Chem. Phys.*, 2012, **14**, 9813.
18 W. Yajun, S. Rui, L. Jie and Z. Yongfa, *Energy Environ. Sci.*, 2011, **4**, 2922.
19 X. Guangcheng, Y. Bing, C. Junyu and Y. Jinhua, *Chem. - Eur. J.*, 2011, **17**, 5145.
20 S. Kumar, B. Kumar, T. Surendar and V. Shanker, *Mater. Res. Bull.*, 2014, **49**, 310.
21 P. Chengsi, X. Jing, W. Yajun, L. Di and Z. Yongfa, *Adv.Funct. Mater.*, 2012, **22**, 1518.